Energies and time-resolved spectroscopy of 10—2000-Å emissions from laser plasmas produced by a picosecond laser

Noboru Nakano* and Hiroto Kuroda
The Institute for Solid State Physics, The University of Tokyo, Minato-ku, Tokyo 106, Japan
(Received 30 October 1985; revised manuscript received 16 December 1986)

Various characteristics of x-ray emission from laser plasmas produced by a picosecond YAG laser (where YAG represents yttrium aluminum garnet) are investigated in the wide wavelength band ranging from 10 to 2000 Å from the point of view that emitted radiation from laser plasmas is applied to many purposes, such as laser fusion, x-ray lasers, x-ray sources, and solid-state physics. In this wide wavelength band, extremely different dependences of x-ray energies on input laser energies are made clear. With a decrease of the wavelength, the slope of the dependences increases. Decay times of emitted x-rays from laser plasmas are approximately proportional to the wavelengths. Computational studies are also performed in the framework of a transient collisional radiative model in order to explain the experimental results.

I. INTRODUCTION

For laser fusion research, x rays from laser-produced plasmas are important diagnostic tools for the estimation of electron temperatures and densities.[1–13] Many investigations have been performed along this line. Laser plasmas are also used as x-ray laser media and many works concerning x-ray laser studies are also reported.[14–18] It has been confirmed experimentally that x rays are amplified in cylindrical laser plasmas.[19] In addition, laser plasmas are important x-ray sources for x-ray lithography, extended x-ray-absorption fine-structure (EXAFS) studies, and other uses.[20–22] For these many purposes, it is important to know the relationship of output x-ray energies to input laser energies and the temporal behavior of x-ray energies as a function of the wavelength of emitted x rays. Several experimental works have reported dependences of x-ray energies or intensities from laser plasmas on input laser energies.[23–28] However, in these works limited x-ray wavelength bands below 12 Å have been investigated using nanosecond ruby lasers and nanosecond CO_2 lasers. Also, many papers[29–37] have been presented concerning temporal behavior of x-ray pulses mainly in the 1.5 to 12 Å range using nanosecond and picosecond lasers. These papers conclude that x-ray pulses follow incident laser pulses. Experimental studies of wavelength bands between 3000 and 7000 Å were reported by Fischer and Kuhne using nanosecond lasers.[38] However, Fischer and Kuhne used duration times of photoemissions that were comparable to the laser pulsewidth and it is doubtful that their measurements were correctly performed. In these works, only limited wavelength regions were investigated using mainly nanosecond lasers.

This paper clarifies the dependences of laser-plasma emitted energies on incident laser energies and the temporal behavior of emitted pulses as a function of emission wavelength using picosecond lasers. In this study, a picosecond laser was used for the following two reasons: (1) As a study of basic physics, we seek the mechanism of x-ray generation from picosecond laser plasmas. To clarify the mechanism, transient ionization processes must be accounted for. For instance, we previously showed that for a low-z aluminum target it takes about a few hundred picoseconds for ionization states to reach equilibrium states for plasmas with 300 eV of electron temperature and about 10^{21} cm^{-3} electron density.[39] In that paper, energies of continuum x rays below 5.4 Å from picosecond laser plasmas could be successfully explained as a function of atomic number of target materials by considering transient ionization processes. In this paper we compare experimental results of x-ray energy dependences on laser energies with computational results. (2) X rays from picosecond laser plasmas have several uses. We expect that the x-ray pulse width decreases and that conversion efficiencies from laser energies to x-ray energies increase because emissions occur mainly before thermal energies are converted to kinetic energies. One of the many uses of x rays from laser plasmas is to make x-ray lasers. As lasing medium and photo-pump sources, x rays from picosecond laser plasmas are important because gain of x-ray lasers lasts a shorter time with decreasing wavelength. For instance, in one paper, the laser pulse width was 500 ps for x-ray amplifications at about 200 Å.[19] To make x-ray lasers with a wavelength less than 200 Å, we must understand dependences of gain and its duration time on wavelength and plasma conditions. As a first step, we intend to clarify decay time of emitted pulses and dependence of emitted energies on input laser energies in the wide wavelength band. As stated above, in previous works limited wavelength bands were investigated using mainly nanosecond lasers. Systematic studies using picosecond lasers in the wide wavelength band ranging from less than 10 to 2000 Å have not been reported. In addition, correct measurements of decay times are only possible using picosecond lasers, because decay times are less than one nanosecond in the band below about 100 Å as can be seen in our data shown below.

A YAG laser (where YAG represents yttrium aluminum garnet) with 30 ps of pulse width and 100 mJ of energy was focused on various targets and emitted x rays

from laser plasmas were measured in the following three selected wavelength ranges: (i) 1200—2000 Å, (ii) 90—110 Å, and (iii) $\lesssim$10 Å. By this selection, important information is thought to be lost in the other wavelength bands. But this lack is completely compensated by the benefit of obtaining a wide range scope. For instance, decay time, and slope of emitted energy dependences on input laser energies, show monotonous variations with wavelength decrease of emitted pulses in three wavelength bands. We suspect that decay time characteristics and slope in the other wavelength bands follow the same monotonous variations. In the band between 15 and 300 Å, measurements can be easily done using the technique in this paper if desired. Detailed works in this range will be performed. In addition, in this band we obtained time-integrated spectra and showed a good agreement with computational results using a transient collisional radiative (CR) model.[40] This model will include different lifetime and rate coefficients concerning emissions in various wavelength bands. It is helpful to predict characteristics in the 15—300-Å band. In the 300—1200-Å band, energy measurement will be done in the near future. It is important to note that, by this selection, we want to get a rough insight on scaling laws concerning temporal decay and dependence of emitted energies on input laser energies as a function of wavelength. From measurements of emitted energies, we obtained the experimental fact that emitted energies show extremely different dependence on input laser energies in the above three wavelength bands, and the slope of dependences is inversely proportional to wavelength. From time-resolved measurements, it is clear that temporal behavior of emitted pulses can be fitted well with a single exponential decay curve and decay times are proportional to wavelength.

To explain temporal behavior of emitted pulses in wavelength band (iii), a set of rate equations was solved using a transient collisional radiative (CR) model. In laser plasmas produced by a picosecond laser, ionization stages change within the pulse width and differ significantly from those under the steady-state condition. Because x rays are generated from ions in transient ionization stages, it is important to note that a computational analysis must be done using a transient CR model. Experimental results concerning dependences of emitted energies on incident laser energies are compared with computational results for the transient CR model in wavelength region (iii). We describe experiments and results in Sec. II, computations and results in Sec. III, and discussions in Sec. IV, respectively.

II. EXPERIMENTS AND RESULTS

A single pulse was emitted from a YAG mode-locked oscillator and amplified by four amplifier stages. This pulse with 30 ps of pulse width and 100 mJ of laser energy was focused on target using a 150-mm focal length lens. Target material was mainly aluminum. The wavelength range was divided into the following three bands: (i) 1200—2000 Å, (ii) 90—110 Å, and (iii) $\lesssim$10 Å. Adequate spectrometers are available for these bands. In the band (i) a vacuum ultraviolet spectrometer (MINUTEMAN, Model 302-VM) equipped with a MgF_2-coated grating (600 gratings/mm) was used. In band (ii) a grazing-incidence spectrometer was used. This spectrometer was developed for precise measurement and a flat-field spectrogram can be easily obtained in the band from 15 to 300 Å.[40] A wide spectral band ranging from 15 to 300 Å can be covered using 30×50 mm^2 gratings with 1200 grooves/mm at 87° incidence angle (30—300 Å) and 2400 grooves/mm at 89° incidence angle (15—150 Å). This spectrometer has the advantage of a flat-focal position, and coupling to two-dimensional detectors such as a micro-channel plate (MCP), a linear diode array, and a streak camera is easily performed. Performance of this spectrometer and applications to plasma spectroscopy are described in Ref. 40. A grating with 1200 grooves/mm is suitable for present experiments performed in the band between 90 and 110 Å. In band (iii) x-ray spectra were obtained by a spectrometer equipped with a KAP (potassium acid phthalate) crystal.

Next, various detectors are described for measurement of emitted energies. A photomultiplier with a MgF_2 window (a rise time of 3 ns, HAMAMATSU PHOTONICS) is used for band (i). A photomultiplier with a plastic scintillator used as a frequency converter from x rays to visible light acts as a simple detector for bands (ii) and (iii). Total sensitivities of the measuring system including spectrometers, windows, scintillators, and photomultipliers are varied as a function of wavelength. But, in this study of three wavelength bands, narrow band spectra were selected. In band (i) the range ±5 Å was selected for the vacuum-ultraviolet spectrometer and the center of spectra was varied from 1200 to 2000 Å. In band (ii) the range ±10 Å centered at 100 Å was selected for the flat-field spectrometer. In the band (iii) the range ±0.5 Å centered at 7.8 Å was selected for the crystal spectrometer. A flat response was assumed in the narrow bands and deconvolution was not necessary to get emitted energies from detector signals. Therefore, measured signals reflect genuine information on emitted energies. Energy spectra are not discussed in this paper. Energy sensitivity of these detectors was checked by varying both the distance between laser plasmas and measurement points and the size of an aperture set on the detectors. For time-resolved spectroscopy, the above photomultiplier with a MgF_2 window has high enough resolution to measure a long decay of emissions with about several tens of ns in band (i). In band (ii) a windowless streak camera with a photocathode of parylene coated with CsI is available. In band (iii), as is widely done, a streak camera uses a Be window coated with Au on the rear surface which acts as a photocathode. Detections of total amount of ions are also carried out by an ion collector. Next, experimental results are presented. First, we describe the dependence of x-ray energies on incident laser energies.

A. Dependence of x-ray energies on incident laser energies

1. 1200—2000 Å

In band (i) emitted energies from various targets show similar dependence on input laser energies. As typical examples, results for C, Al, and Sm at 1200 Å are shown in Fig. 1. In the whole band from 1200 to 2000 Å, similar

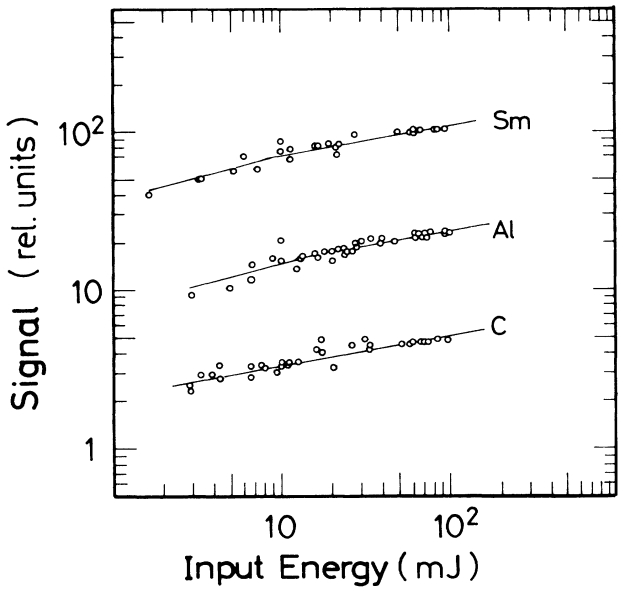

FIG. 1. Dependence of measured signals at 1200 Å on input laser energies. The results for C, Al, and Sm targets are shown.

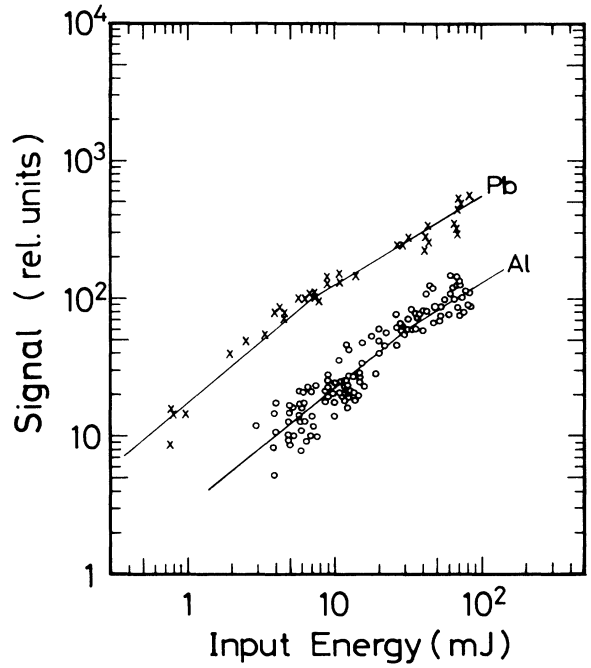

FIG. 2. Dependence of measured signals at 100±10 Å on input laser energies. The results for Al and Pb targets are shown.

dependences to curves in Fig. 1 are obtained. Curves are plotted in this figure in relative units for ease of viewing, and relations in strength among the three targets have no meaning. Because spectra from Sm targets consist of many x-ray lines and can be regarded as quasicontinuum spectra, data for this target appear to be important from the standpoint of many applications as x-ray sources. As shown in Fig. 1, results for the three targets show similar dependences, which can be summarized simply as $E \propto E_{\text{in}}^{0.2-0.4}$.

2. 90–110 Å

The spectrum range near 100 Å attracted keen interest from the viewpoint of x-ray lasers. For instance, x-ray amplification was reported at about 200 Å, and it is proposed that x-ray lines near 100 Å using $2s^2$-$2s4p$, $4p$-$3d$, and $4f$-$3d$ transitions can be used as the pumping source and possible x-ray laser sources.[41] The spectral range between 90 and 110 Å can be selected from the flat-field spectral band between 30 and 300 Å using a 1200 grooves/mm grating by inserting a slit in front of a detector. In the other bands between 15 and 300 Å, measurements can be easily done in the same way using the two gratings (1200 and 2400 grooves/mm) described in this paper if desired. Typical results for Al and Pb targets obtained in band (ii) are shown in Fig. 2. The two graphs are drawn in relative units to be easily seen. Data fluctuations of the results for Al targets appear to be larger than those for Pb targets. The origin of fluctuations will be discussed in Sec. III. From results for various targets such as Fe, Ni, and Pb, including the above data for Al and Pb targets, dependences of emitted energies can be summarized simply as $E \propto E_{\text{in}}^{0.66-0.85}$. It appears of interest to investigate x-ray energies as a function of atomic

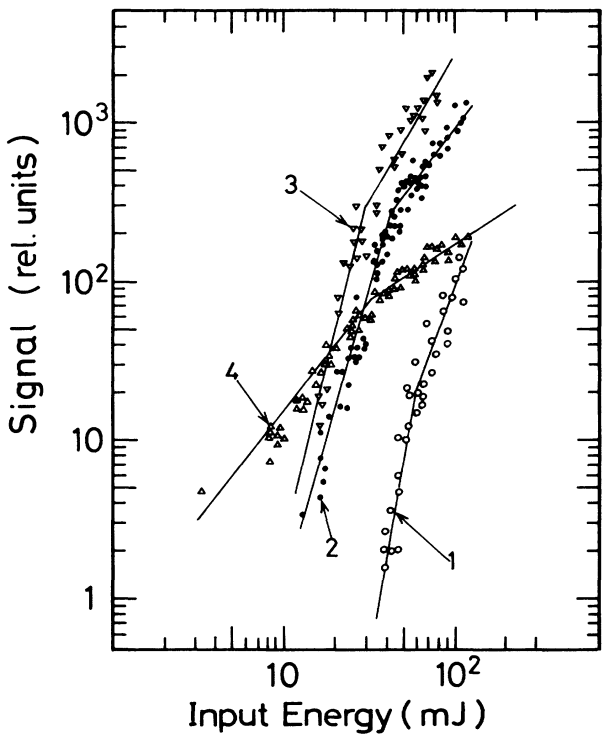

FIG. 3. Dependence of x-ray measured signals at about 7.8 Å on input laser energies. 1, signals of line x rays; 2, signals of continuum x rays less than 8.2 Å through Be filter with thickness of 30 μm; 3, signals of continuum x rays less than 3.1 Å through Be filter with thickness of 500 μm; 4, ion collector signals.

TABLE I. Dependences of x-ray energies in various x-ray regions on input energies or electron temperatures.

		Experiments		Computations		Normalized computational results	
	E_1 (mJ)	$E_{in} < E_1$	$E_1 < E_{in}$	$T_e < 500$ eV	500 eV $< T_e$	$T_e < 500$ eV	500 eV $< T_e$
1200 Å		$E_{in}^{0.2-0.4}$					
100±10 Å	30	$E_{in}^{0.85}$	$E_{in}^{0.66}$				
8 Å[a]	60	$E_{in}^{6.2}$	$E_{in}^{2.9}$	T_e^{9} ($E_{in}^{6.0}$)	$T_e^{4.6}$ ($E_{in}^{3.1}$)	$E_{in}^{6.7}$	$E_{in}^{3.8}$
8.2 Å[b]	40	$E_{in}^{3.7}$	$E_{in}^{1.4}$	T_e^{4} ($E_{in}^{2.7}$)	$T_e^{1.6}$ ($E_{in}^{1.1}$)	$E_{in}^{3.4}$	$E_{in}^{1.8}$
3.1 Å[c]	30	$E_{in}^{4.4}$	$E_{in}^{1.8}$				

[a]Line x rays set behind a crystal spectrometer (from curve 1 in Fig. 3).
[b]Continuum x rays through Be filter with thickness of 30 μm (from curve 2 in Fig. 3).
[c]Continuum x rays through Be filter with thickness of 500 μm (from curve 3 in Fig. 3).

number in view of applications of laser plasmas as an x-ray source. These data will be published in another article.[42]

3. $\lesssim 10$ Å

Figure 3 shows emitted energies from aluminum plasmas in band (iii). Curve 1 presents data obtained using a plastic scintillator coupled to a photomultiplier as the detector in a crystal spectrometer. These data are integrated values over the band 7.8±0.5 Å as a function of wavelength. In this band x-ray spectra are measured by a crystal spectrometer equipped with a KAP crystal. A typical spectrum is shown in Fig. 4. From this figure, line x-ray energy due to the transition $1s2p\ ^{1,3}P-1s\ ^2S$ in Al heliumlike ions can be seen to be strongest compared to other energies of line and continuum x rays. Using the same type of detector, x-ray energies through Be filters with thicknesses of 30 and 500 μm were also measured. These data are presented as curves 2 and 3. These curves are drawn in relative units and relations in strength among these curves have no meaning. Among these curves, the slope of curve 1 is sharpest. From these curves, dependences of x-ray energies can be obtained. For instance, dependences of x-ray energies E of curve 1 can be written as $E \propto E_{in}^{2.9}$ in the high-energy side larger than 55 mJ and $E \propto E_{in}^{6.2}$ in the low-energy side less than that energy. These results are summarized in Table I. In the experimental series, fast ions could not be observed. This can be explained by reasons such as low energies of input lasers and incident beam polarization (s polariza-

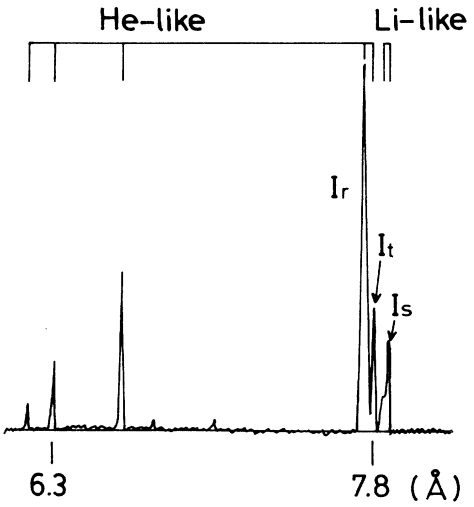

FIG. 4. X-ray spectra measured by a crystal spectrometer (from Ref. 39).

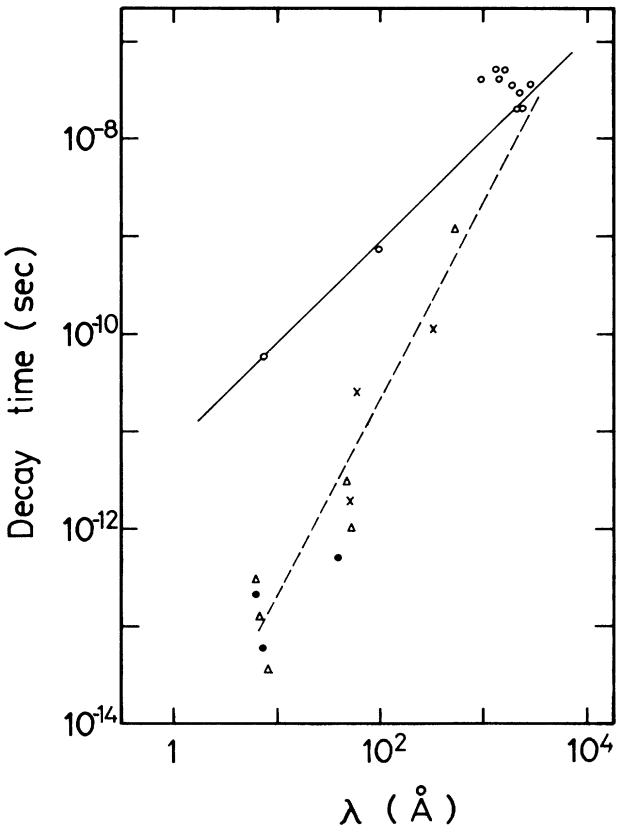

FIG. 5. Measured decay times as functions of wavelengths are shown as open circles. The other symbols denote theoretical values for radiative lifetimes for the transition of atomic levels.

tion). In Fig. 3 time-integrated ion collector signals are represented by curve 4 in order to estimate x-ray energies from computational results. Because pulse widths of ion collector signals do not vary with increasing input laser energies, time-integrated signals nearly represent peak values of ion collector signals.

B. Temporal behavior of emitted pulses in the wavelength band from 10 to 2000 Å

In this series of experiments, aluminum targets were mainly used. Results for various targets in band (ii) are presented in another paper.[42] Temporal behavior of x-ray energies in band (i) was measured and it showed slow decay of several tens of nanoseconds. Therefore, in this band, correct measurements can be easily done using a photomultiplier with a MgF_2 window and a 3-ns rise time. Rise times of signals are determined by the time response of the photomultiplier, whereas decay times vary from 20 to 50 ns irregularly as functions of wavelengths ranging from 1200 to 2000 Å. Details will be published elsewhere. In bands (ii) and (iii) two types of streak cameras are available to correctly measure decay curves of less than 1 ns.

In band (ii) rise time of x-ray signals between 90 and 110 Å follows the laser pulse waveform, whereas signals show slightly long decay time of about 800 ps compared to a laser pulsewidth of about 30 ps. This decay time is obtained by fitting the energy decay curve with a single exponential decay. In band (iii) rise time is also determined by the laser and decay time of about 70 ps is slightly longer than laser pulse width. This decay time is of the same order as laser pulse width and deconvolution is necessary. Experimental results concerning decay times described above are plotted in Fig. 5 as open circles and appear to be fitted well by a solid line. The other symbols (●, △, and ×) denote theoretically obtained optical transition times. Difference between measured decay times and optical transition times increases with decrease of x-ray wavelength. It appears of interest to note that decay times of x-ray pulses are approximately proportional to wavelength of x rays.

III. COMPUTATIONS AND RESULTS

In computations, x-ray lines in band (iii) are treated, because in this region energies of x-ray lines depend most sharply on input laser energies. In addition, in experimentally obtained spectra x-ray lines are clearly assigned[39] and comparison between experimental and computational results can be performed correctly. Many computer simulations concerning x-ray emission from laser plasmas were reported.[43–52] For instance, in Refs. 50 and 52, radiation transport in laser-heated foil targets was treated and x-ray spectra at the front side and the rear side of the foil were obtained. Owing to these works, x-ray emission from laser plasmas were completely modelized. However, in these works, nanosecond lasers were mainly considered for applications to laser fusion. In our previous paper,[39] we estimated the time for ionization states to come into equilibrium for plasmas with constant electron temperatures. For instance, for aluminum at 300 eV of electron temperature and about 10^{21} cm^{-3} of electron density, the time is about a few hundred picoseconds. Therefore, in picosecond-laser plasmas we must take into account the effect of ionization processes in calculations of x-ray energies. In that paper we reported that experimental results of continuum x rays as a function of atomic number could be explained well by computational results based on this model.[39] In our other articles,[12,13] it is made clear that careful attention must be paid when intensity ratios of x-ray lines are used as the diagnostic method for estimates of electron temperatures and densities. The framework of the model in this paper is the same as the previously reported one. That is, in our model, we adopted transient plasmas in an ionizing phase produced and sustained by a picosecond laser. In our computations, the following assumptions were made for simplicity: (1) Electron temperatures, T_e, keep constant values supplied from laser light during ionization processes. A laser pulse width of 30 ps is vastly longer than the electron-electron collision time of about 3×10^{-14} sec ($n_e\sim10^{21}$ cm^{-3}, $Z\sim10$, $T_e\sim500$ eV). Therefore, electron temperatures are determined by the balance between absorption and loss. In this assumption, input laser energy is considered to vary so as to make up for the loss. Although this assumption is thought to be far from the situation in the experiment, we accept this assumption for convenience to compare transient solutions with steady-state ones. (2) Total ion densities, including neutral particles, are kept at constant values because plasma does not expand during the laser pulse-width interval. Ion population densities in a ground state $n_{\alpha,0}$ and an excited state $n_{\alpha,1}$ distributed in each charge state ($0\le\alpha\le Z$) can be calculated by solving the following equations:

$$
\begin{aligned}
dn_{\alpha,0}/dt &= -n_{\alpha,0}n_e[C_{i,\alpha}(0)+R_{r,\alpha-1}(0)+n_eD_{i,\alpha-1}(0)] \\
&\quad +n_{\alpha+1,0}n_e[R_{r,\alpha}(0)+n_eD_{i,\alpha}(0)]+n_{\alpha-1,0}n_eC_{i,\alpha-1}(0)\ . \\
dn_{\alpha,1}/dt &= n_{\alpha,1}\left[\sum_m -\{n_e[D_{e,\alpha}(m,l)+C_{e,\alpha}(l,m)]+R_{d,\alpha}(l,m)\}-n_eC_{i,\alpha}(l)-A_{i,\alpha}(l)\right] \\
&\quad +\sum_m \{n_e[D_{e,\alpha}(l,m)+C_{e,\alpha}(m,l)]+R_{d,\alpha}(m,l)\}n_{\alpha,m} \\
&\quad +n_e[n_eD_{i,\alpha}(l)+E_{c,\alpha}(l)+R_{r,\alpha}(l)]n_{\alpha+1,0} \\
&= 0\ ,
\end{aligned}
$$

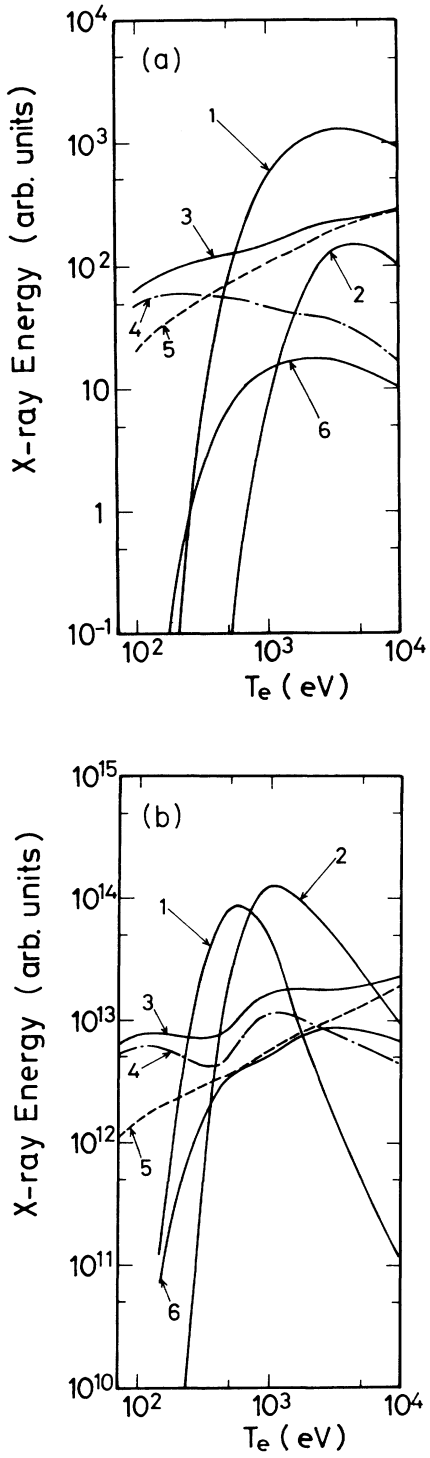

FIG. 6. (a) and (b) show x-ray energies calculated in the framework of a transient CR model and a steady-state CR model, respectively. 1, a resonance line $1s2p$-$1s^2$ from aluminum heliumlike ions; 2, a resonance line $2p$-$1s$ from aluminum hydrogenlike ions. Lines 3, 4, 5, and 6 denote continuum x rays due to free-free (ff) and free-bound (fb) transitions. Lines 3, 4, and 5 are energy values after integration of wavelengths (w). 3, continuum x rays $(\mathrm{ff}+\mathrm{fb})_w$; 4, continuum x rays $(\mathrm{fb})_w$; 5, continuum x rays $(\mathrm{ff})_w$; 6, continuum x rays $(\mathrm{ff}+\mathrm{fb})_{8\ \text{Å}}$.

where $R_{d,\alpha}(l,m)$ is a radiative decay rate,[53] $C_{e,\alpha}(l,m)$ $[D_{e,\alpha}(m,l)]$ is a collisional excitation (deexcitation) rate,[2,4,5,47,54–58] $A_{i,\alpha}(l)$ is an autoionization rate,[53] $E_{c,\alpha}(l)$ is an electron capture rate,[53] $R_{r,\alpha}(l)$ is a radiative recombination rate,[43,45,47] and $C_{i,\alpha}(l)$ $[D_{i,\alpha}(l)]$ is a collisional ionization (three-body recombination) rate,[43] respectively. Levels included in our calculations are listed in Table II. In future, analysis will be performed in the other x-ray bands. Validity of assuming quasiequilibrium for excited states was already argued by Mewe and Schrijver.[59] Details were written in our previous paper.[13] As initial conditions, we take the value of f_1 $(=n_1/\sum_i n_i)$ as 10^{-3}, f_0 $(=n_0/\sum_i n_i)=1-f_1$, $f_j=0$ $(2\le j\le Z)$. The value of n_0 is determined by the condition that n_e is 10^{21} cm^{-3} at 30 ps, where n_0 and n_1 denote neutral densities and singly charged ion densities, respectively.

Next, computational results are presented. X-ray energies in Fig. 6(a) are obtained after temporal integration of time-dependent values in the transient CR model during the laser pulse width. For comparison, results for a steady-state CR model are shown in Fig. 6(b). In these figures, curves 1 and 2 present energies due to resonance transitions of Al XII $1s2p$-$1s^2$ and Al XIII $2p$-$1s$, respectively. Energies of continuum x rays due to free-free and free-bound transitions are indicated by curves 4 and 5, respectively. Curve 3 shows total amount of continuum x-ray energies. These continuum x-ray energies show values also integrated along wavelengths. Curve 6 presents the total amount of continuum x-ray energy at about 8 Å calculated for comparison with x-ray line energies.

The following facts are drawn after comparison of results in Fig. 6(a) with those in Fig. 6(b).

(1) For any electron temperatures, x-ray line energies from the Al XIII ions represented by curve 2 are not larger than those from Al XII ions represented by curve 1 in the framework of a transient CR model. This fact is at odds with results for a conventional steady-state CR model.

(2) Values of electron temperatures at which x-ray energies are at maximum increase when computations are performed in a transient CR model instead of a steady-state CR model.

IV. DISCUSSION

A. Dependences of x-ray energies on input laser energies

1. Experimental results

Experimentally obtained dependences of emitted energies on input laser energies in three wavelength regions are shown in Table I. It is important to note that slope of dependences increases monotonously with decrease of wavelength.

2. Computational results at about 8 Å and comparison with experimental results

In Sec. IV A 2 (a) difference of computational results between steady-state solutions and transient ones are described. It is also shown that transient solutions are

TABLE II. Levels included in our calculations.

Aluminum ions	Levels
Hydrogenlike ion	$1s,2p,3p,4p,5p$
Heliumlike ion	$1s^2\,{}^1S;1s2p\,{}^1P,{}^3P;1s3p\,{}^1P,{}^3P;1s4p\,{}^1P,{}^3P;1s5p\,{}^1P,$ $^3P;1s2s\,{}^1S,{}^3S;2s2p\,{}^1P,{}^3P;2p^2\,{}^3P,{}^1D,{}^1S$
Lithiumlike ion	$1s^22s^2S;1s^22p^2P;1s(2s2p\,{}^1P)^2P,1s(2s2p\,{}^3P)^2P;$ $1s2p^2\,{}^2P,{}^2D$

consistent with experimentally obtained x-ray spectra. In Sec. IV A 2 (*b*) temperature-dependent computed results are converted to energy-dependent ones to compare computational results with experimental ones.

(*a*) As was described in Sec. II concerning computational results for x-ray line energies near 8 Å, different points between steady-state solutions and transient ones can be summarized as follows: (i) energy of a resonance line from heliumlike ions takes larger values than that from hydrogenlike ions for any electron temperatures in a transient CR model; (ii) electron temperatures, at which x-ray line energies take a maximum value, increase when computations are performed in a transient CR model instead of a conventional steady-state CR model. These results are brought about by an ionization state which differs vastly from that in the steady state and by the number of hydrogenlike ions which are much fewer than heliumlike ions within the 30 ps of the laser pulse width.

Next, the following experimental result is explained by the computation. That is, compared to energies of a resonance line from heliumlike ions (I_{He}), those from hydrogenlike ions (I_{H}) are too weak to be observed. Accounting for the dynamic range of sensitivities of x-ray films, intensity ratio $R=I_{\mathrm{H}}/I_{\mathrm{He}}$ is estimated as less than 10^{-2}. In the series of experiments, maximum electron temperatures were measured at about 700 eV. Based on computational results for 700 eV of electron temperature, intensity ratio R is obtained as $O(1)$ for the steady-state solutions and less than $O(10^{-2})$ for the transient solutions. Therefore, experimentally obtained spectra are consistent with transient solutions.

(*b*) Temperature dependences in the computational results are changed to input laser energy dependences by using the following relations described below. From plasma front velocities (v) measured by ion collectors and the relationship $v\propto T_e^{1/2}$, electron temperatures T_e are determined to be proportional to $E_{\mathrm{in}}^{0.67}$. This result agrees well with previously reported relations.[60] Using this relationship, x-ray energies can be written as functions of input laser energies from Figs. 6(a) and 6(b). These results are shown in the parentheses of computational results in Table I.

Next, note that in computations total ion numbers (N_t) including neutral number is assumed to be constant. But, in experiments, numbers N_t increase with increase of input laser energies. Therefore, the normalized value, the product of computationally obtained energies, and N_t is compared to experimental results. For this purpose, we consider the signal of ion collectors. Signal S can be written as $S\propto\sum_i Z_iN_i=\langle Z\rangle N_t$, where $\langle Z\rangle$ and N_t denote an average charge state and a total ion number, respectively. In this equation, dependences of signal of ion collectors on input laser energies are determined by those of both $\langle Z\rangle$ and N_t. We intend to draw dependences of N_t on energies from ion collector signals using computational results. Experimentally, electron temperatures T_e can be obtained from continuum x-ray spectra measured using Be thin-foil filters of various thicknesses (100, 200, 330, and 430 μm) as shown in our previous paper[39] and those values are determined as about 500 eV for input energies E_{in} of 30 mJ. For those values of T_e, $\langle Z\rangle$ takes about 10 in the computational results. Because aluminum has atomic number 13, $\langle Z\rangle$ depends weakly on E_{in} for energies above 30 mJ. Therefore, dependences of ion collectors signals on E_{in} shown by curve 4 in Fig. 3 are determined mainly by those of N_t for energies above 30 mJ. We believe that the bend of the ion signals at 30 mJ is brought about by the extreme change of $\langle Z\rangle$ with decrease of E_{in}, and N_t depends on E_{in} similarly at both the high-energy region above 30 mJ and the low-energy region. Using N_t obtained above, dependences of normalized x-ray energies on input laser energies are shown in Table I. These computational results should be compared with the experimental ones and, as shown in the table, both results agree well. It is important to note that experimental results concerning dependences of x-ray energies on input energies can be explained by computational ones for the transient CR model.

3. *Comparison of our results with previously reported ones*

Several experimental works have been reported concerning dependences of x-ray energies or intensities from laser plasmas on input energies.[23–29] These works investigated x-ray band (iii) at about 10 Å using nanosecond ruby lasers and nanosecond CO_2 lasers. Results of these works are shown in Table III. These results can be summarized as $E_{\mathrm{x\ ray}}\propto E_{\mathrm{in}}^{2.5\pm0.5}$ except data No. 2. This dependence can be compared with our result at 8.2 Å of Table I. The power 2.5 ± 0.5 is between 3.7 at the low-energy side and 1.4 at the high-energy side of Table I. It is interesting to note that energy dependence of a picosecond laser approaches that of a nanosecond laser with increasing input laser energy at about 10 Å.

B. Dependences of decay times on wavelength of emitted x-rays

As was described in Sec. II, decay times show irregular changes ranging from 20 to 50 ns as a function of wave-

TABLE III. Dependences of x-ray energies on laser energies (E_{in}) previously reported.

	Ref.	Laser	Target	Wavelength (Å)	Dependence
1. P. E. Dyer	23	CO_2, 60 ns, 1.2×10^{11} W/cm^2	Al,C,$(CH_2)_n$, Pb,Ag,Cu	8.8[a]	$E_{in}^{2.5-2.8}$
2. M.C. Richardson	24	CO_2, 1.5 ns, 10—50 J	Al	8.8[a]	$E_{in}^{1.3}$
3. H. Pepin	25	CO_2, 1.8 ns, 4 J	C,Fe,Sn, Pb,Al	8.8[a]	$E_{in}^{2.3}$
4. D. J. Nagel	26	ruby, 18 ns, 10 J	Mg	12	$E_{in}^{2.4}$
5. R. D. Bleach	27	ruby, 21 ns, 9 J	Al	8.2[b]	$E_{in}^{2.5}$
6. T. W. Johnston	28	CO_2, 1.2—1.5 ns, 10 J	$(CH_2)_n$	8.8[a]	$E_{in}^{2.1}$
			Al	8.2[b]	$E_{in}^{2.5}$

[a]Through Be windows with 25 μm thickness.
[b]Through Be windows with 30 μm thickness.

lengths of emissions between 1200 and 2000 Å. Compared to spectra, it is made qualitatively clear that in the band with long decay times a number of x-ray lines gather and in the other band with short decay times continuum x-ray energies are dominant. Irregular changes of decay times are shown on the upper right side of Fig. 5.

Next, we describe decay times in the bands at about 100 Å and at 10 Å. From the spectrograph in the band around 100 Å, line x rays are dominant in this wavelength region[40] and measured decay times are about 800 ps, which is long compared to laser pulse width. Long decay time is determined by temporal behavior of x-ray lines. To measure temporal change of continuum x rays, decay curves for the Sn target were also measured. In spectra, energies of continuum x rays for Sn are stronger than those for Al. The measured decay curve can be fitted well with two exponentials. Slow decay time was about 110 ps and fast decay was about laser pulse width. Because fast decay vanishes in the other x-ray band, where x-ray line energies are dominant, it can be concluded that observed fast decay is brought about by continuum x rays. In the band at about 10 Å, a Be filter 30 μm thick is used as a window. Both line x rays and continuum ones can go through this window. However, in x-ray spectra obtained by a crystal spectrometer equipped with the same window, line x rays appear to be dominant in comparison with continuum x rays also in this spectral band as shown in Fig. 4. In the band below 10 Å, decay time of continuum x rays seems to be about laser pulse width as in the band from 90 to 110 Å, because continuum x rays with short wavelength emit from hotter plasma regions than those with short wavelength do. This idea is supported by experiments by Key *et al.*,[61] who showed that continuum x rays at about 6 Å had the same duration time as laser pulse width (100 ps). Therefore, although energies of continuum and line x rays were not measured, in this band, decay time of about 70 ps seems to be determined also by temporal behavior of line x rays.

Measured decay times ranging from 10 to 2000 Å are plotted on Fig. 5 as open circles. From these plots, it is shown that decay times are simply proportional to wavelengths. This dependence differs extremely from dependence of a radiative lifetime τ_R, for transition of atomic levels as a function of wavelength λ which can be simply written as $\tau_R \propto \lambda^2$. Difference increases with decrease of wavelength. This difference exists because x-ray emis-

TABLE IV. Decay times or pulse width of x rays previously reported.

	Ref.	Laser	Target	Wavelength (Å)	Decay time or pulse width
1. G. I. Brukhnevitch	29	Nd:Glass, 10 ps, 1—2 J	Ti	5.7[a]	~60 ps
2. H. G. Ahlstrom	30	Nd:Glass, 70 ps, 28 J	Glass shell	3.1—4.8	~120 ps
3. J. D. Kilkenny	31	Nd:Glass, 0.6 ns,	Pt on plastic	~6.2	~3 ns
		2ω, 0.35 ns, 5×10^{14} W/cm^2		1.5—2.5	~2 ns
4. B. Yaakobi	32	Nd:Glass, 40—80 ps, 16 GW	Glass shell	3.1—12	~150 ps
5. M. H. Key	33	Nd:Glass, 100 ps, 15—45 J	Al on glass or	7.8[b]	~300 ps
			glass shell	10[c]	~200 ps
6. G. L. Stradling	34	Nd:Glass, 700 ps, 3×10^{13} W/cm^2	Au disk	18,62	~1 ns
7. R. L. Kauffman	35	Nd:Glass, 900 ps, $\sim10^{15}$ W/cm^2	Si,Al disk	~7.8[b]	~900 ps
8. H. G. Ahlstrom	36	Nd:Glass, 135 ps, 42.4 J,	Glass shell	4.8	~120 ps
		52 ps, 15.5 J			70 ps
9. E. M. Campbell	37	Nd:Glass, 1 ns, $\sim1\times10^{14}$ W/cm^2	Au	0.18—0.41	$\lesssim$1 ns

[a]Through Be window with 100 μm thickness.
[b]Al XII $1s^2$-$1s2p$ ^1P, ^3P.
[c]Ne X L_β.

sions occur during plasma expansions through recombination processes, and decay times are determined by decrease of electron temperatures, densities, and total magnitude of recombination processes concerning emitted line x rays. Other systematic measurements support this explanation. Details will be published elsewhere.[42] Taking into account time scales of measured decay times, these measurements are made possible only by using picosecond lasers. Although it was pointed out experimentally and theoretically that photoemissions from laser plasmas occur during plasma expansions through recombination processes,[11,12,62,63] dependence of decay times on wavelengths has been measured for the first time.

Next, our results are compared with previously reported ones. Many works are presented concerning temporal behavior of x-ray energies in band from 1.5 to 12 Å.[29–37] Results of these works are listed in Table IV. Key *et al.*[33] observed long decay of line x rays compared with laser pulse. Laser pulse width of 30 ps used in our work is between 10 and 70 ps listed at no. 1 and no. 2 of Table IV and our measured decay time for aluminum targets, 70 ps, is also similar to results of no. 1 and no. 2, in which different targets were used. Although it is concluded in most other papers listed in this table that x-ray pulses followed laser pulse waveform, this observation comes from long laser pulse width relative to x-ray pulses. In the band from 3000 to 7000 Å, experiments using a nanosecond laser are presented.[38] In that paper, decay times of photoemission pulses with several tens of nanoseconds similar to our data are measured and increase proportionally with increasing laser pulse width. These decay times are comparable with laser pulse width and it is doubtful that decay times were measured correctly.

V. CONCLUSION

Various characteristics of x-ray emissions from laser plasmas were investigated in wide wavelength bands from 10 to 2000 Å. This wide wavelength band was divided into the following three regions: (i) 1200—2000 Å, (ii) 90—110 Å, and (iii) $\lesssim$10 Å. Laser plasmas were produced by focusing a YAG laser with 30-ps pulse width and 100 mJ on various targets. Dependences of emitted energies from laser plasmas on input laser energies and dependences of decay times on wavelengths of emitted energies were measured for the first time. In the band (i), (ii), and (iii), a vacuum-ultraviolet spectrometer (MINUTEMAN, Model 302-VM), a newly developed grazing incidence spectrometer, and a spectrometer equipped with a KAP crystal were used, respectively. Computational studies were also performed to explain experimental results at around 8 Å. Results can be summarized as follows.

(1) In bands (i), (ii), and (iii), extremely different dependences of x-ray energies on input laser energies were made clear. With decrease of wavelength, slope of dependences increases.

(2) Computational results were compared with experimental ones concerning dependences of x-ray energies on input laser energies in band (iii). Experimentally obtained dependences can be explained well by results in a transient CR model. Results in a conventional steady-state CR model were far from the experimental ones. Intensity ratio I_H/I_{He} between resonance line intensity of a hydrogenlike ion (I_H) and that of a heliumlike ion (I_{He}) can also be explained by results in a transient CR model.

(3) Decay times of emitted x rays from laser plasmas are approximately proportional to wavelengths in wide bands ranging from 10 to 2000 Å. This experimental fact was obtained for the first time using a picosecond YAG laser.

Results are important from the viewpoint that emitted radiations from laser plasmas are used for many purposes such as laser fusion, x-ray lasers, and x-ray sources in solid-state physics.

---

*Present address: New Material Research Center, High Technic Lab., Kawasaki Steel Corp., Kawasaki-cho, Chiba City, Chiba 260, Japan.

[1]A. H. Gabriel and T. M. Paget, J. Phys. B **5**, 673 (1972).
[2]A. H. Gabriel, Mon. Not. R. Astron. Soc. **160**, 99 (1972).
[3]C. R. Bhalla, A. H. Gabriel, and L. P. Prenyakov, Mon. Not. R. Astron. Soc. **172**, 359 (1975).
[4]E. V. Aglitskii, V. A. Boiko, A. V. Vinogradov, and E. A. Yukov, Kvant. Elektron. (Moscow) **1**, 579 (1975) [Sov. J. Quantum Electron. **4**, 322 (1974)].
[5]A. V. Vinogradov, I. Yu. Skobelov, and E. A. Yukov, Kvant. Elektron (Moscow) **2**, 1165 (1975) [Sov. J. Quantum Electron. **5**, 630 (1975)].
[6]E. V. Aglitskii, A. N. Zherikhin, P. G. Kryukov, and S. V. Chekalin, Zh. Eksp. Teor. Fiz. **46**, 1344 (1977) [Sov. Phys.—JETP **46**, 707 (1977)].
[7]I. Yu. Skobelov, A. V. Vinogradov, and E. A. Yukov, Phys. Scr. **18**, 78 (1978).
[8]V. A. Boiko, S. A. Pikuz, and A. Ya. Faenov, J. Phys. B **12**, 1889 (1979).
[9]A. V. Vinogradov, I. Yu. Skobelov, and E. A. Yukov, Usp. Fiz. Nauk **129**, 177 (1979) [Sov. Phys.—Usp. **22**, 771 (1979)].
[10]J. Dubau and S. Volonte, Rep. Prog. Phys. **43**, 199 (1980).
[11]V. A. Boiko, A. Ya. Faenov, S. Ya. Hahalin, S. A. Pikuz, K. A. Shilov, and I. Yu. Skobelov, J. Phys. B **16**, L77 (1983).
[12]N. Nakano and H. Kuroda, Phys. Rev. A **29**, 3447 (1984).
[13]N. Nakano and H. Kuroda, Appl. Phys. Lett. **45**, 130 (1984).
[14]F. E. Irons and N. J. Peacock, J. Phys. B **7**, 1109 (1974).
[15]P. Jaegle, G. Jamelot, A. Carillon, A. Sureau, and P. Dhez, Phys. Rev. Lett. **33**, 1070 (1974).
[16]R. J. Dewhurst, D. Jacoby, G. J. Pert, and S. A. Ramsden, Phys. Rev. Lett. **37**, 1265 (1976).
[17]V. A. Bhagavatula, IEEE J. Quantum Electron. **QE-16**, 603 (1980).
[18]D. Jacoby, G. J. Pert, S. A. Ramsden, L. D. Shorrock, and G. J. Tallents, Opt. Commun. **37**, 193 (1981).
[19]D. L. Matthews, P. L. Hagelstein, M. D. Rosen, M. J. Eckart, N. M. Ceglio, A. U. Hazi, H. Medecki, B. J. MacGowan, J. E. Trebes, B. L. Whitten, E. M. Campbell, C. W. Hatcher, A. M. Hawryluk, R. L. Kauffman, L. D. Pleasance, G. Rambach, J. H. Scofield, G. Stone, and T. A. Weaver, Phys. Rev. Lett. **54**, 110 (1985).

[20]*Laser-Induced Fusion and X-Ray Laser Studies,* edited by S. F. Jacobs, M. O. Scully, M. Sargent, and C. D. Cantrell (Addison-Wesley, Reading, MA, 1976).
[21]P. J. Mallozzi and R. E. Schwerzel, Science **206**, 353 (1979).
[22]Rutherford Appleton Laboratory Annual Report to the Laser Facility Committtee, 1984 (unpublished).
[23]P. E. Dyer, S. A. Ramsden, J. A. Sayers, and M. A. Skipper, J. Phys. D **9**, 373 (1976).
[24]M. C. Richardson, N. H. Burnett, H. A. Baldis, G. D. Enright, R. Fedosejevs, N. R. Isenor, and I. V. Tomov, in *Laser Interaction and Related Plasma Phenomena,* edited by H. J. Schwarz and H. Hora (Plenum, New York, 1977), Vol. 4A, p. 176.
[25]H. Pépin, B. Grek, F. Rheault, and D. J. Nagel, J. Appl. Phys. **48**, 3312 (1977).
[26]D. J. Nagel, R. R. Whitlock, J. R. Greig, R. E. Pechacek, and M. C. Peckerar, Proc. SPIE Int. Soc. Opt. Eng. **135**, 46 (1978).
[27]R. D. Bleach and D. J. Nagel, J. Appl. Phys. **49**, 3832 (1978).
[28]T. W. Johnston, H. Pépin, F. Martin, B. Grek, P. Church, J. Geoffrion, J. C. Kieffer, J. P. Matte, G. Mitchel, and R. Decoste, in *Laser Interaction and Related Plasma Phenomena,* edited by H. J. Schwarz, H. Hora, M. J. Lubin, and B. Yaakobi (Plenum, New York, 1981), Vol. 6, p. 246.
[29]G. I. Brukhnevitch, V. K. Chevokin, Yu. S. Kasyanov, V. V. Korobkin, A. A. Malyutin, A. M. Prokhorov, M. C. Richardson, M. Ya. Schelev, and B. M. Stepanov, Phys. Lett. **51A**, 249 (1975).
[30]Ref. 24, p. 437.
[31]Ref. 28, p. 483.
[32]B. Yaakobi, D. Steel, E. Thorsos, A. Hauer, B. Perry, S. Skupsky, J. Geiger, C. M. Lee, S. Letzring, J. Rizzo, T. Mukaiyama, E. Lazarus, G. Halpern, H. Deckman, J. Delettrez, J. Soures, and R. McCrory, Phys. Rev. A **19**, 1247 (1979).
[33]M. H. Key, C. L. S. Lewis, J. G. Lunney, A. Moore, J. M. Ward, and R. K. Thareja, Phys. Rev. Lett. **44**, 1669 (1980).
[34]G. L. Stradling, Ph.D. thesis, University of California, 1982.
[35]R. L. Kauffman, D. L. Matthews, J. D. Kilkenny, R. W. Lee (unpublished).
[36]H. G. Ahlstrom, in *Laser Plasma Interaction,* edited by R. Balian and J-C. Adam (North-Holland, Amsterdam, 1982), p. 245.
[37]E. M. Campbell, C. E. Max, M. D. Rosen, D. W. Phillion, R. E. Turner, K. Estrabrook, B. Lasinski, W. L. Kruer, and W. C. Mead, in *Laser Interaction and Related Plasma Phenomena,* edited by H. Hora and G. H. Miley (Plenum, New York, 1984), Vol. 6, p. 555.
[38]J. Fischer and M. Kuhne, Appl. Phys. B **32**, 157 (1983).
[39]N. Nakano and H. Kuroda, Phys. Rev. A **27**, 2168 (1983).
[40]N. Nakano, H. Kuroda, T. Kita, and T. Harada, Appl. Opt. **23**, 2386 (1984).
[41]M. Krishnar and J. Trebes, Appl. Phys. Lett. **45**, 189 (1984).
[42]N. Nakano and H. Kuroda, Phys. Rev. A (to be published).
[43]D. Colombant and G. F. Tonon, J. Appl. Phys. **44**, 3524 (1973).
[44]K. G. Whitney and J. Davis, Appl. Phys. Lett. **24**, 509 (1974).
[45]D. G. Colombant, K. G. Whitney, D. A. Tidman, N. K. Winsor, and J. Davis, Phys. Fluids **18**, 1687 (1976).
[46]D. Salzmann and A. Krumbein, J. Appl. Phys. **49**, 3229 (1978).
[47]D. Duston and J. J. Duderstadt, J. Appl. Phys. **49**, 4388 (1978).
[48]H. D. Shay, R. A. Haas, W. L. Kruer, M. J. Boyle, D. W. Philion, V. C. Rupert, H. N. Kornblum, F. Rainer, V. W. Slivinsky, L. N. Koppel, L. Richards, and K. G. Tirsell, Phys. Fluids **21**, 1634 (1978).
[49]J. D. Perez and G. L. Payne, Phys. Rev. A **21**, 968 (1980).
[50]D. Duston and J. Davis, Phys. Rev. A **23**, 2603 (1981).
[51]D. Duston, R. W. Clark, J. Davis, and J. P. Apruzese, Phys. Rev. A **27**, 1441 (1983).
[52]D. Duston, R. W. Clark, and J. Davis, Phys. Rev. A **31**, 3220 (1985).
[53]L. A. Vainshtein and V. I. Safronova, At. Data Nucl. Data Tables **21**, 49 (1978).
[54]O. Bely, Proc. Phys. Soc., London **88**, 587 (1966).
[55]R. Mewe, Astron. Astrophys. **20**, 215 (1972).
[56]J. Davis, J. Quant. Spectrosc. Radiat. Transfer **14**, 549 (1974).
[57]R. K. Landshoff and J. D. Perez, Phys. Rev. A **13**, 1619 (1976).
[58]J. D. Perez, J. Appl. Phys. **48**, 1969 (1977).
[59]R. Mewe and J. Schrijver, Astron. Astrophys., Suppl. Ser. **33**, 115 (1978).
[60]T. P. Hughes, *Plasmas and Laser Light* (Hilger, London, 1975), p. 386.
[61]M. H. Key, C. L. S. Lewis, J. G. Lunny, A. Moore, J. M. Ward, and R. K. Thareja, Phys. Rev. Lett. **44**, 1669 (1980).
[62]M. K. Matzen and J. S. Pearlman, Phys. Fluids **22**, 449 (1979).
[63]P. K. Carrol, E. T. Kennedy, and G. O. Sullivan, Appl. Opt. **19**, 1454 (1980).